

Article

Gas Content and Gas Occurrence Mechanism of Deep Coal Seams in the Shenfu-Linxing Block

Litao Ma ^{1,2}, Fan Yang ^{3,*}, Jianghao Yang ^{1,2}, Yi Cui ⁴, Wei Wang ^{1,2}, Cheng Liu ^{1,2}, Bo Zhang ^{1,2}, Jiang Yang ^{1,2} and Shu Tao ^{5,*}

¹ CNOOC EnerTech-Drilling & Production Co., Tianjin 300452, China; malt@cnooc.com.cn (L.M.); yangjh38@cnooc.com.cn (J.Y.); wangwei193@cnooc.com.cn (W.W.); liucheng14@cnooc.com.cn (C.L.); zhangbo53@cnooc.com.cn (B.Z.); jiangyang4@cnooc.com.cn (J.Y.)

² CNOOC Energy Technology & Services Limited Key Laboratory for Exploration & Development of Unconventional Resources, Tianjin 300452, China

³ PetroChina Research Institute of Petroleum Exploration and Development, Beijing 100083, China

⁴ Zhalainuoer Coal Industry Co., Ltd., Hulunbuir 021410, China; cuiyicugb@126.com

⁵ School of Energy Resources, China University of Geosciences (Beijing), Beijing 100083, China

* Correspondence: yangfan84@foxmail.com (F.Y.); taoshu@cugb.edu.cn (S.T.)

Abstract: The Shenfu-Linxing block in the Ordos Basin holds abundant deep coalbed methane (CBM) resources, which can alleviate gas shortages and aid dual carbon target achievement. Considering isothermal adsorption traits and parameters like vitrinite reflectance, temperature, pressure, and water saturation, a prediction model for adsorbed and free gas content was formulated. This model helps to reveal the deep CBM occurrence mechanism in the Shenfu-Linxing block. Results show that deep CBM exists in both adsorbed and free states, with adsorbed gas initially increasing then decreasing, and free gas rising then stabilizing as burial depth increases. A critical transition depth for total CBM content exists, shallowing with higher water saturation. As depth increases, temperature and pressure evolution results in a “rapid growth—slow growth—stability—slow decrease” pattern in total gas content. Adsorbed gas resides in micropores, while free gas occupies larger pores.

Keywords: prediction model; gas content; coalbed methane; occurrence characteristics



Academic Editor: Reza Rezaee

Received: 14 January 2025

Revised: 29 January 2025

Accepted: 29 January 2025

Published: 3 February 2025

Citation: Ma, L.; Yang, F.; Yang, J.; Cui, Y.; Wang, W.; Liu, C.; Zhang, B.; Yang, J.; Tao, S. Gas Content and Gas Occurrence Mechanism of Deep Coal Seams in the Shenfu-Linxing Block. *Energies* **2025**, *18*, 699. <https://doi.org/10.3390/en18030699>

Copyright: © 2025 by the authors. Licensee MDPI, Basel, Switzerland. This article is an open access article distributed under the terms and conditions of the Creative Commons Attribution (CC BY) license (<https://creativecommons.org/licenses/by/4.0/>).

1. Introduction

The composition of gas in deep coal reservoirs primarily consists of adsorbed and free gas [1–7]. The measured gas content in coal seams is mainly composed of desorption gas, residual gas, and escaping gas. At present, the test samples used are mainly obtained through rope coring. Alternatively, during the process from drilling to loading into the desorption tank, a significant decrease in pressure will result in significant gas loss, especially for deep coal reservoirs rich in free gas. Therefore, the estimated gas loss is usually much lower than the actual gas loss, resulting in low total gas content test results [8–11]. In recent years, pressure maintaining coring technology has significantly improved the accuracy of gas content testing. However, it remains challenging to quantitatively measure the free gas content [12,13]. Many scholars have developed prediction models for deep CBM content using methods such as principal component analysis, isothermal adsorption techniques, and adsorption potential theory [12,14–19]. Nevertheless, the research focus is mainly on relatively shallow coal reservoirs, lacking quantitative characterization of gas content in deep coal seams.

In contrast to traditional shallow coal reservoirs, the geological characteristics of deep coal reservoirs, including high stress, high temperature, and high pressure, result in considerable alterations in the pore structure of coal, ultimately causing substantial variations in the occurrence state of CBM [2,20,21]. As burial depth increases, the quantity of adsorbed gas increases and subsequently decreases, whereas the quantity of free gas progressively rises. The content of free gas is also affected by the level of water saturation [1,15,22]. In deep coal reservoirs, both adsorbed gas and free gas coexist, with a distinct “critical depth” serving as a separator between them. Above this critical depth, a notable positive pressure effect is observed, leading to an augmentation in the adsorbed gas content as the burial depth increases [22–24]. Beyond the depth, the negative effect of temperature becomes significant. Thus, as the burial depth increases, the negative effect of temperature intensifies, while the positive effect of pressure gradually weakens. As a result, the amount of adsorbed gas decreases progressively, while the amount of free gas rises. While free gas and adsorbed gas both exist in deep coal reservoirs, adsorbed gas continues to dominate in terms of overall proportion [25–28]. Conversely, when water saturation diminishes and burial depth intensifies, the content of free gas has the potential to exceed that of adsorbed gas. Generally, low-rank deep coal reservoirs contain a relatively free gas content, while medium- and high-rank deep coal reservoirs still have a high proportion of adsorbed gas [29–33].

To quantify the CBM content of different phases in deep coal seams and improve prediction accuracy, this study established prediction models for adsorbed gas and free gas content based on high-temperature and high-pressure isothermal adsorption experiments. By combining the Langmuir model, the evolution characteristics and occurrence mechanism of methane in different phases of deep coal reservoirs were revealed.

2. Geological Setting

The Ordos Basin, a significant intra-cratonic basin situated in North China, holds the second-largest coal resource reserves in the country [34] (Figure 1a). The basin is segmented into seven structural subdivisions [35,36] (Figure 1b). The Shenfu-Linxing area is situated at the central-eastern fringe of the Ordos Basin, bordered by the Baode region to the north and the Sanjiaobei area to the south (Figure 1c). It spans the northern slope of Shaanxi and the western Shanxi fold belt in structure. The internal structure is relatively complex, with locally developed small faults and folds, and multiple secondary structural units. The Shenfu-Linxing block mainly develops strata such as Ordovician Majiagou Formation (O_{1m}), Carboniferous Benxi Formation (C_{2b}), Taiyuan Formation (C_{3t}), Shanxi Formation (P_{1s}), Permian Lower Shihezi Formation (P_{2x}), Upper Shihezi Formation (P_{2s}), Shiqianfeng Formation (P_{3sh}), Triassic Liujiagou Formation (T_{1l}), Heshanggou Formation (T_{1h}), Zhifang Formation (T_{2z}), Yanchang Formation (T_{3y}), and Quaternary System (Q). Among them, Taiyuan Formation and Shanxi Formation contain a significant number of coal seams. At present, the No. 8+9 coal seam of Taiyuan Formation is the key layer for deep CBM exploration and development in the entire region (Figure 2).

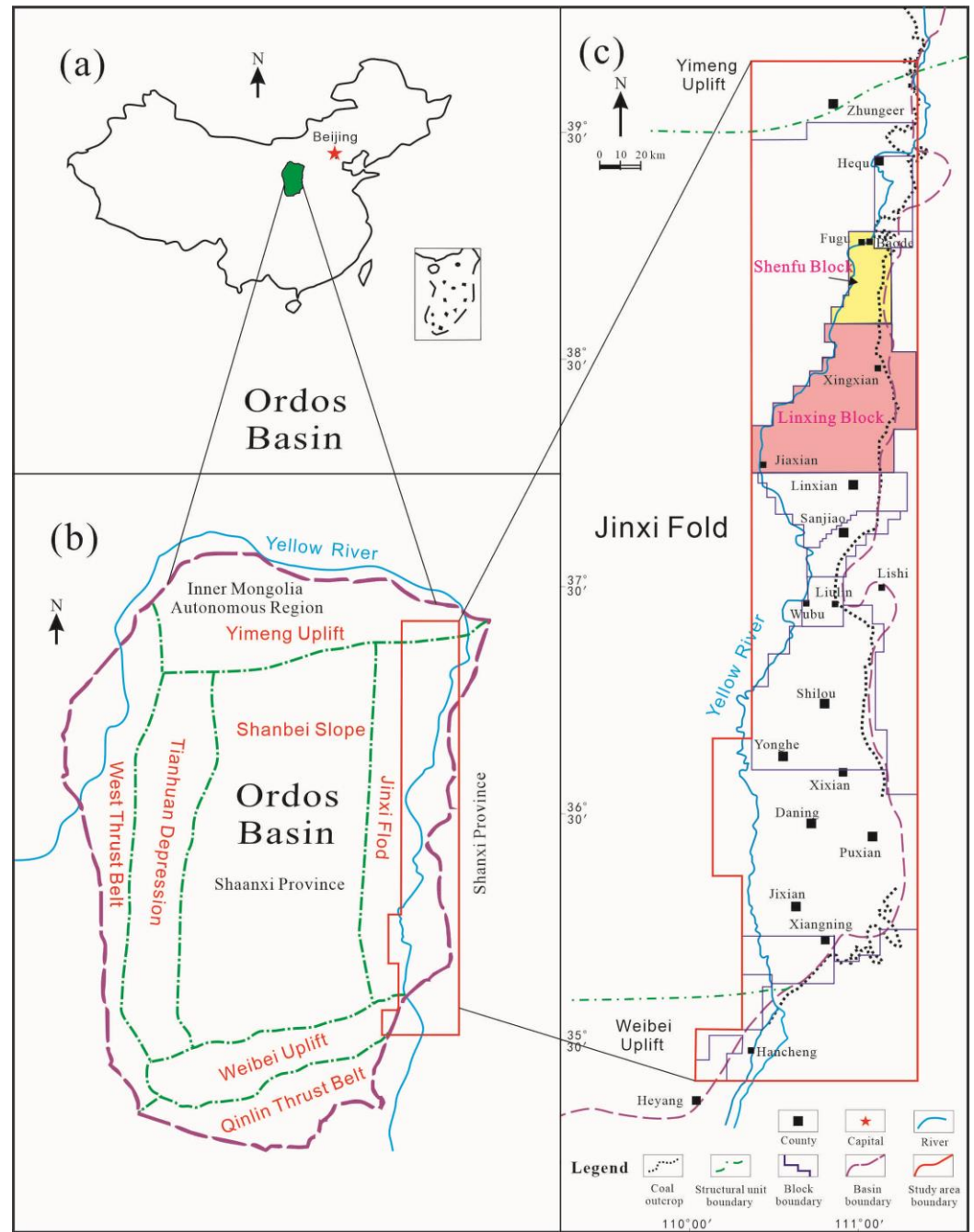


Figure 1. (a) Location of the Ordos Basin; (b) Tectonic units of the Ordos Basin; (c) Division of eastern margin of Ordos Basin and the location of Shenfu-Linxing block (modified from [37]).

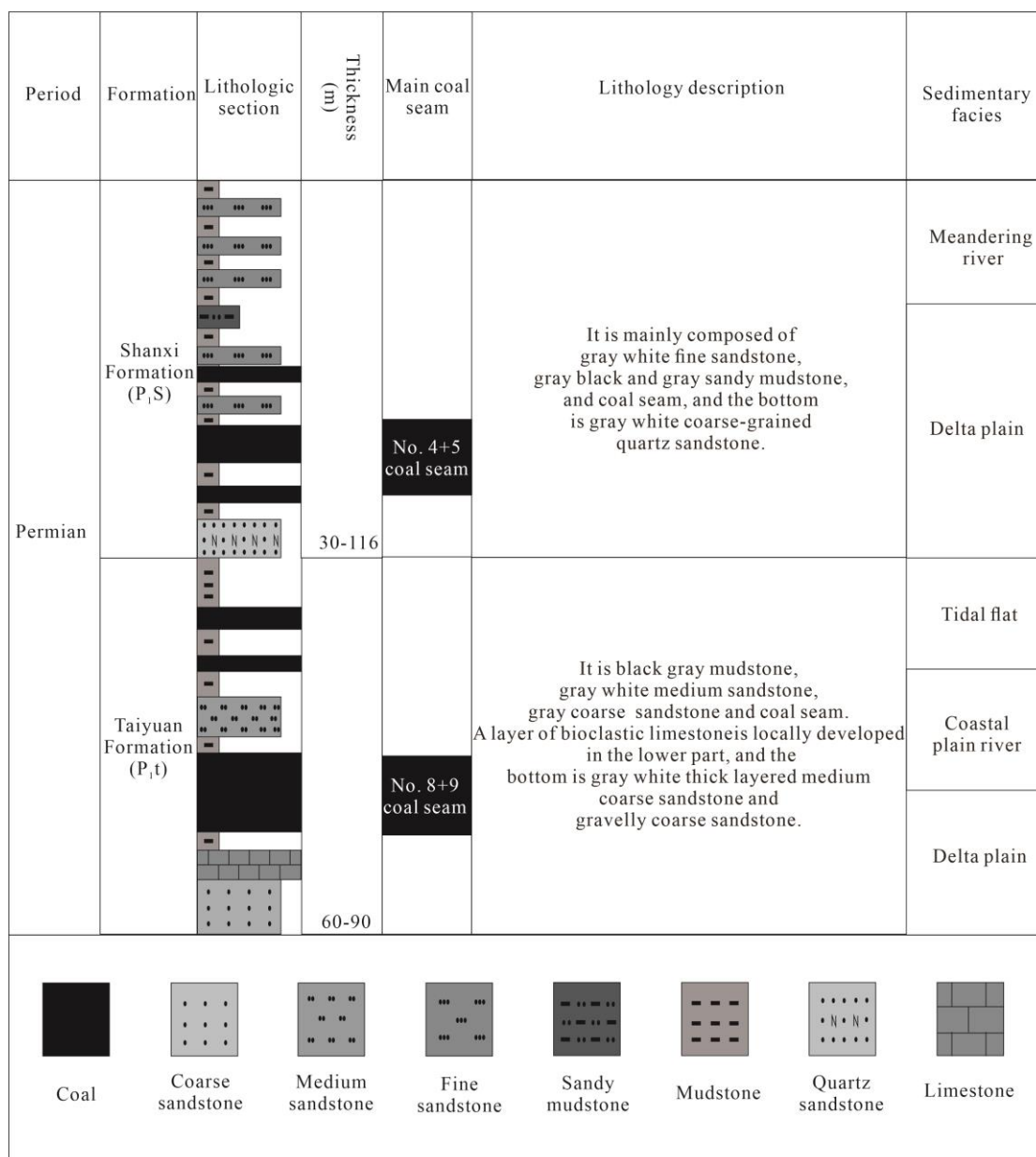


Figure 2. Lower Permian stratigraphic column in the Shenfu-Linxing block (modified from [37]).

3. Experiments and Methods

3.1. Material Composition

Six coal samples were taken from the No. 8+9 coal seam in the Shenfu-Linxing block, with a sampling depth of 1968–2344 m. All of the samples were used to conduct proximate analysis tests and microscopic component tests following the Chinese national standard GB/T 30732-2014 [38] and GB/T 8899-2013 [39], respectively. Meanwhile, the vitrinite reflectance (R_o) of the coal samples was tested according to GB/T 6948-2008 [40].

3.2. Isothermal Adsorption Test

According to the national standard GB/T 19560-2008 [41], adsorption tests were performed under varying temperature and pressure conditions to analyze isothermal behavior. To further understand the mechanism by which temperature affects methane adsorption capacity, the temperature points were set as 30 °C, 50 °C, and 70 °C, with a maximum pressure of 30 MPa.

3.3. Gas Content Prediction Methods

The Langmuir adsorption equation (Equation (1)) is a single-molecule layer adsorption theoretical model, which is an isothermal equation obtained from the adsorption system in dynamic equilibrium. It is widely used to calculate the amount of adsorbed gas in coal [42,43].

$$V = \frac{P \cdot V_L}{P + P_L} \quad (1)$$

where, V is the methane adsorption capacity of the coal, cm^3/g ; P_L is the Langmuir pressure, MPa; V_L is the Langmuir volume, cm^3/g ; P is the reservoir pressure, MPa.

When the reservoir temperature is above $20\text{ }^\circ\text{C}$ and the gas pressure is less than 20 MPa, it can be considered as an ideal gas state. Therefore, the calculation of free gas content can be based on the ideal gas state equation (Equations (2) and (3)).

$$\frac{P_0 V_0}{T_0} = \frac{P V_1}{T} \quad (2)$$

$$P = \frac{\rho R T}{M} \quad (3)$$

where, P_0 represents the standard gas pressure, which is 0.101 MPa; V_0 is the gas volume under standard conditions, m^3 ; T_0 is the absolute temperature, 273.15 K; P is the reservoir pressure, MPa; V_1 is the volume of free gas, m^3 ; T is the actual reservoir temperature, K; ρ is the gas density, kg/m^3 ; R is the Avogadro constant; M is the molar mass of the gas.

By combining the general gas state equation [44] and the Boyle Malotte law [45], the final equation for calculating free gas is obtained (Equation (4)).

$$V_1 = \frac{K(\Phi - \Phi_w)}{\rho_1} \quad (4)$$

where, V is the volume of free gas, m^3 ; K is the porosity stress attenuation coefficient; Φ is the porosity of the coal reservoir, %; Φ_w is the porosity occupied by water, %; ρ_1 is the measured apparent density of coal, t/m^3 .

4. Results and Discussion

4.1. Basic Information of Coals

The primary macrolithotype of coal in the Shenfu-Linxing block is semi-bright coal, with a relatively complete coal structure. The basic information of coal samples is shown in Table 1. The R_o of coal samples varies from 0.95% to 1.33%, belonging to medium-rank coal. According to proximate analysis results, the moisture content, ash yield, and volatile matter account for 0.8–2.44%, 8.71–29.74%, and 13.21–30.41%, respectively. The vitrinite group has the highest content in the macerals (63.7–91.3%), followed by the inertinite group (8.6–36.2%), while the exinite group is basically undeveloped.

Table 1. Results of the proximate and maceral analyses.

Sample No.	Coal Seam No.	Depth (m)	R_o (%)	Maceral Composition (%)			Proximate Analysis (%)			
				Vitrinite	Inertinite	Exinite	M_{ad}	A_{ad}	V_{ad}	FC_{ad}
lx1	8+9	1968.4–1969.3	1.25	90.6	9.3	0.1	0.84	29.74	15.41	54.01
lx2	8+9	1980.8–1981.1	1.2	72.5	27.5	/	2.44	27.91	13.21	56.44
lx3	8+9	2004.3–2004.9	1.33	63.7	36.3	/	1.33	10.41	18.14	70.12
sm1	8+9	2135.1–2135.4	1.25	91.2	8.8	/	0.80	8.71	25.61	64.88
sm2	8+9	2235.2–2235.5	1.19	81.3	18.6	0.1	1.06	11.33	20.14	67.47
sm3	8+9	2343.9–2344.1	0.95	84.3	15.4	0.3	1.35	9.68	30.41	58.56

Notes: M_{ad} is moisture content; A_{ad} is ash yield; V_{ad} is volatile yield; FC_{ad} is fixed carbon content; ad is air-dried basis.

4.2. Isothermal Adsorption Characteristics

As depicted in Figure 3, there is a notable positive relationship observed between pressure and Langmuir volume. As the burial depth increases, the pressure of the coal reservoir rises, leading to an increase in Langmuir volume and enhanced coal adsorption capacity.

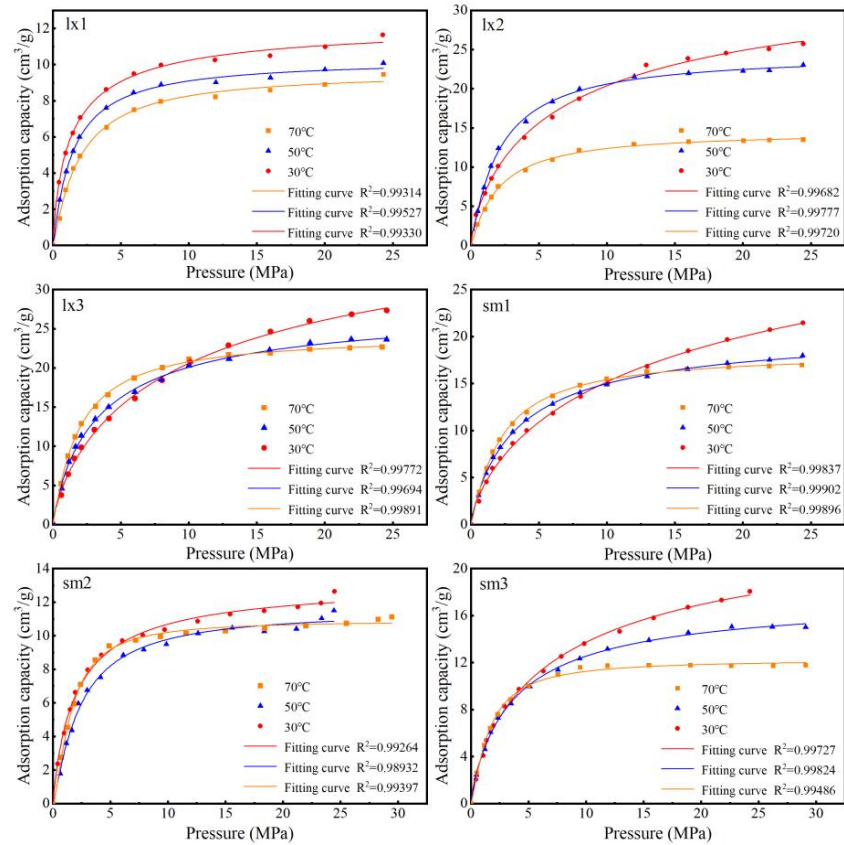


Figure 3. Characteristic diagram of isothermal adsorption curves under different temperatures (30 °C, 50 °C, 70 °C) and pressure conditions in the Shenfu-Linxing block.

In the range of low pressure (0–5 MPa), an abrupt and substantial increase in the coal's adsorption capacity is observed as pressure rises, suggesting a strong influence of pressure on the coal's adsorption capacity during this phase. Nevertheless, in the medium-pressure range, the rate of increase in adsorption capacity significantly diminishes (5–10 MPa). In the high-pressure section (>10 MPa), the adsorption capacity of the coal gradually reaches a plateau, indicating that in deep coal seams under high pressure, the influence of pressure on the coal's adsorption capacity becomes less significant [46,47].

The V_L of coal is 11.97–32.30 m^3/t , and the P_L is 1.49–4.79 MPa. As the temperature increases, the V_L decreases (Table 2), and the adsorption capacity of the coal decreases at the same pressure (Figure 3). However, in the low-pressure range, the adsorption capacity does not vary significantly with temperature, as evidenced by the overlapping isotherm adsorption lines. Hence, at shallower burial depths, the effect of temperature on adsorption capacity is comparatively minor. As the burial depth increases, in the medium- to high-pressure section, the adsorption capacity is significantly affected by temperature.

Therefore, the adsorption capacity of the in situ coal seam is jointly controlled by the temperature and pressure of the formation. Pressure has a positive impact on the adsorption capacity of coal, while temperature has a negative impact on it [48]. Under the combined influence of temperature and pressure, the adsorption capacity is predominantly controlled by the pressure in the low-pressure region. As the burial depth increases, the

negative effect of temperature begins to emerge, and the coal samples quickly reach their maximum adsorption capacity under high-temperature conditions, resulting in a reduction of P_L (Table 2).

Table 2. V_L and P_L values of coal samples under different temperature and pressure conditions.

Sample No.	30 °C		50 °C		70 °C	
	V_L	P_L	V_L	P_L	V_L	P_L
lx1	11.97	1.49	10.61	1.60	10.20	2.12
lx2	29.57	4.18	25.00	2.19	14.73	2.11
lx3	32.30	5.58	26.35	2.99	24.63	2.01
sm1	26.45	6.75	19.83	3.12	18.91	2.34
sm2	12.84	1.95	12.02	2.56	11.68	1.70
sm3	20.50	4.55	16.82	3.26	12.93	1.66

4.3. Gas Content Characteristics

4.3.1. Adsorbed Gas Content

Based on the Langmuir model, an improved prediction equation for the adsorption gas volume in the Linxing-Shenfu block was built. Conversely, the R_o of the collected coal samples varies slightly, ranging from 0.95% to 1.33%, and the data are limited (Table 1). To enhance the precision of the model's data fitting, isothermal adsorption experimental data from other blocks in Eastern Ordos Basin, such as Baode, Liulin, and Hancheng, were collected and used.

As illustrated in Figure 4, the relationship between P_L and temperature adheres to an exponential function. Meanwhile, the relationship between P_L and the maximum R_o displays a "U"-shaped trend, initially decreasing and then increasing as the maximum R_o rises. Furthermore, V_L exhibits a linear positive relationship with the maximum R_o and a negative relationship with temperature.

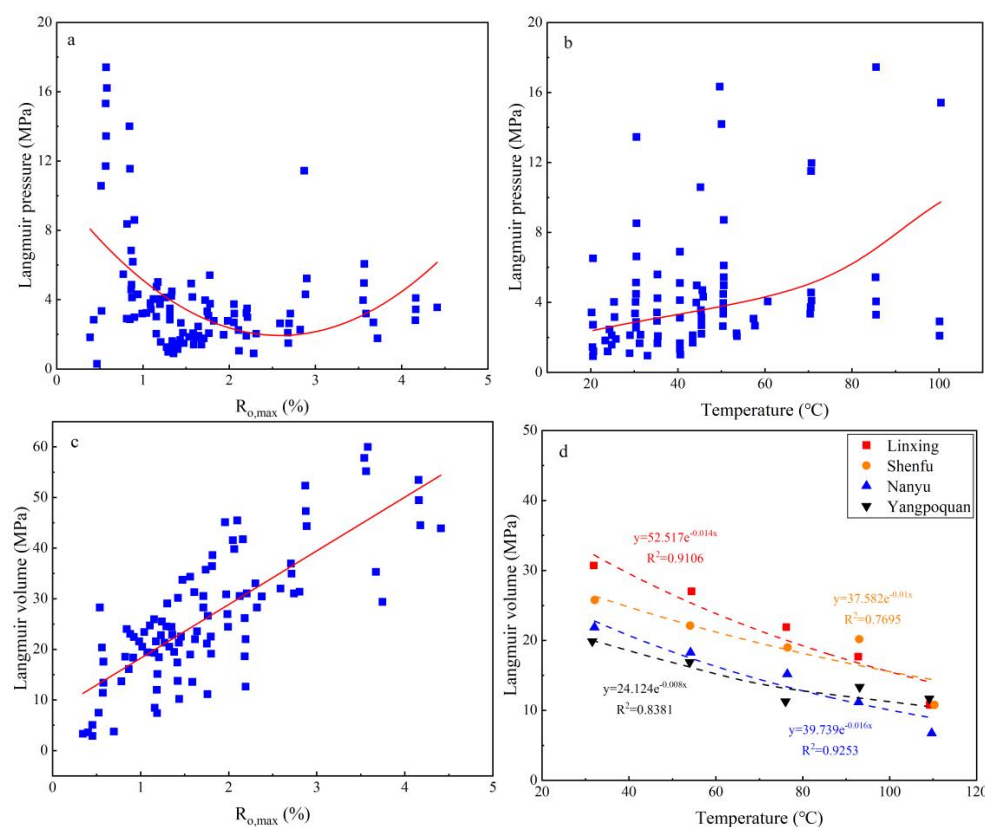


Figure 4. (a) Relationship between Langmuir pressure and $R_{o,max}$; (b) Relationship between Langmuir pressure and temperature; (c) Relationship between Langmuir volume and $R_{o,max}$; (d) Relationship between Langmuir volume and temperature.

According to the isothermal adsorption experimental data, combined with the analysis of the interactions and correlations between the single factors mentioned above, a nonlinear analysis method is used to improve the Langmuir equation and establish a prediction equation for the Langmuir constant (Equations (5) and (6)).

$$V_L = (13.89R_{o,max} + 11.97)e^{-0.0071T} R^2 = 0.83 \quad (5)$$

$$P_L = (0.71R_{o,max} - 3.58R_{o,max} + 5.52)e^{0.014T} R^2 = 0.67 \quad (6)$$

The above equation is brought into the Langmuir equation to obtain the prediction model of adsorbed gas volume suitable for the Shenfu-Linxing block (Equation (7)).

$$V = \frac{P(13.89R_{o,max} + 11.97)e^{-0.0071T}}{P + (0.71R_{o,max} - 3.58R_{o,max} + 5.52)e^{0.014T}} \quad (7)$$

Provided that the geothermal and pressure gradients within the Shenfu-Linxing block remain consistent, with a pressure gradient of 0.9 MPa/hm, a geothermal gradient of 2.4 °C/hm, and a surface temperature of 20 °C, it is possible to determine the adsorbed gas volume for different R_o values and burial depths. Eight samples with measured gas content from the Shenfu-Linxing block were selected to validate the prediction model for adsorption gas content, and the results are summarized in Table 3. The predicted adsorbed gas content is 2.86–15.28 m³/t. The error rates ranged from −4.81% to −25%, with an average error rate of −17.19%. The main reason for this error is the presence of free gas in deep coal reservoirs, which results in predicted adsorbed gas content being lower than the measured total gas content. The difference between the two basically represents the content of free gas (0.72–5.09 m³/t). The observed free gas content is notably minimal, aligning with the expected low levels of free gas typically found in environments with restricted porosity under in situ conditions [11].

Table 3. Validation of prediction model for adsorbed gas content.

Sample No.	Depth (m)	R_o (%)	Measured Total Gas Content (m ³ /t)	Predicted Adsorbed Gas Content (m ³ /t)	Error Rate (%)
L1	2086.65	1.32	15.04	14.32	−4.81
L2	1786	1.33	16.39	14.98	−8.58
L3	1855.7	1.22	17.24	13.81	−19.92
L4	1800.9	1.11	15.78	12.86	−18.52
S1	1923.7	1.32	18.09	14.63	−19.11
S2	2157.9	1.44	20.37	15.28	−25.00
S3	2027.2	1.38	19.29	15.00	−22.26
S4	2029.3	1.41	18.94	15.27	−19.35
Average					−17.19

4.3.2. Free Gas Content

The average porosity of coal in the Shenfu-Linxing block is 4%, with an average apparent density of 1.46 t/m³, and a stress decline coefficient of 1. Figure 5 illustrates the variation of free gas content with burial depth and water saturation. With greater burial depth, the free gas content shows a progressive rise, though the rate of increase diminishes over time. This pattern suggests that while deeper layers contain more free gas, the growth rate is tempered by factors like reduced coal porosity at greater depths. On the other hand, higher water saturation levels lead to a decline in free gas content. At 100% water saturation, the free gas content reaches 0 m³/t, indicating that all pores are filled with water and no free gas remains.

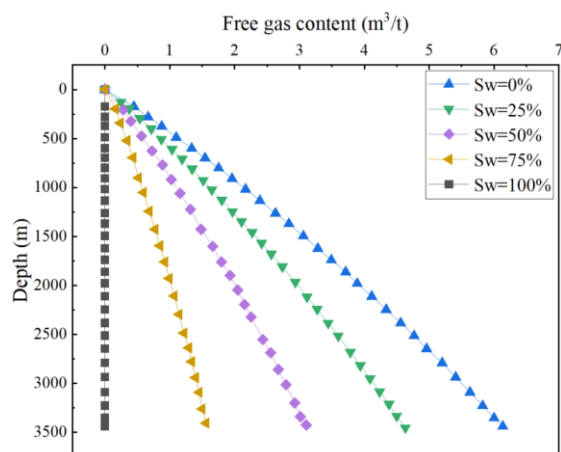


Figure 5. Variation of free gas content with depth.

4.3.3. Dynamic Coupling of Methane Content in Different Phase States

Based on the predictive models for adsorbed and free gas, a clear relationship exists between the total gas content in the coal reservoir of the Shenfu-Linxing block and its depth. As depicted in Figure 6, the saturated adsorption capacity rises initially with greater burial depth before eventually declining. The depth at which the gas content of coal reaches its peak before gradually declining with further burial is referred to as the critical transition depth, which is influenced by factors such as the geothermal gradient, porosity, water saturation, and in situ stress. The overall gas content and the critical transition depth are determined by the interplay between adsorbed and free gas at specific burial depths. Adsorbed gas exhibits a distinct critical transition depth, whereas free gas content shows a linear rise as burial depth increases [49]. Additionally, with rising water saturation in deep coal seams, the adsorbed gas content steadily declines while the free gas content rises, leading to a shallower critical transition depth (Figure 6).

4.4. CBM Occurrence Mechanism

4.4.1. Occurrence Mechanism of Adsorbed Gas

Adsorbed gas can occur in pores through two modes: single-layer adsorption and micropore filling. The theoretical single-layer adsorption capacity is derived from the specific surface area and volume of the pores. By comparing this theoretical adsorption capacity (TAC) with the actual single-layer adsorption capacity obtained from isothermal adsorption experiments, it can be determined whether the adsorbed gas occurs primarily through single-layer adsorption or micropore filling.

Hypothesis I. The gas is completely adsorbed by a single layer in the pores. Based on the single-layer adsorption theory, the TAC can be calculated by the following equation (Equation (8)).

$$V_{tm} = \frac{SSA}{A_m \cdot N_a} \times 22.4 \times 1000 \quad (8)$$

Hypothesis II. The gas is completely contained in the pores in the form of micropore filling. According to the microporous filling theory, the TAC can be determined using the following formula (Equation (9)).

$$V_{tp} = \frac{PV}{V_{mo} \cdot N_a} \times 22.4 \times 1000 \quad (9)$$

where, V_{tm} is the theoretical adsorption gas volume of single layer, m^3/t ; V_{tp} is the theoretical adsorption gas volume of micropore filling, m^3/t ; SSA is the specific surface area of pores, m^2/g ; PV is the pore volume, m^3/g ; A_m is the area occupied by a single methane molecule, $1.134 \times 10^{-19} m^2$; V_{mo} is the volume occupied by a single methane molecule, $2.873 \times 10^{-29} m^3$; N_a is the Avogadro constant, 6.02×10^{23} .

For Hypothesis I, Figure 7 shows that the micropore adsorption capacity closely matches the TAC. This suggests that the micropores in the deep coal reservoirs of the Shenfu-Linxing block provide the main adsorption sites for methane. For Hypothesis 2, the micropore adsorption capacity is basically slightly higher than the theoretical adsorption capacity, and the mesopore adsorption capacity is low, far lower than the theoretical adsorption capacity.

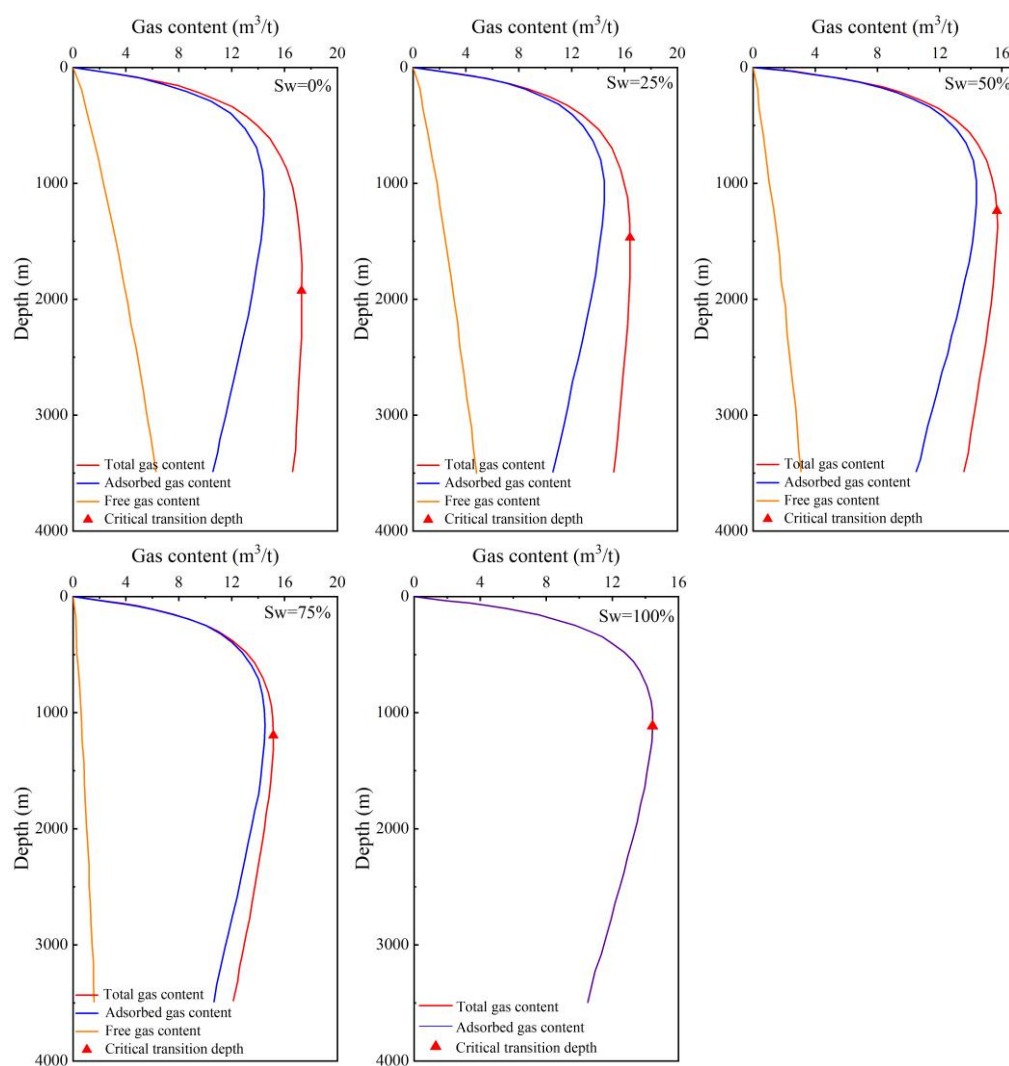


Figure 6. Variation of gas content and critical transition depth with burial depth of coal seam under different water saturation conditions.

Integrating the adsorption potential theory, the adsorption potential on solid surfaces is primarily influenced by curvature. The micropore curvature is the largest in micropores, mesopores, and macropores, and the adsorption potential energy is the highest. The microporous surface exhibits a strong adsorption potential, favoring the adsorption of methane molecules [18]. Thus, when sufficient adsorption space is available, methane molecules are primarily stored in micropores through a filling mechanism. According to

the calculation model, adsorbed gas is characterized by methane molecules exclusively occupying micropores in a filled state, with no such filling observed in mesopores [50,51].

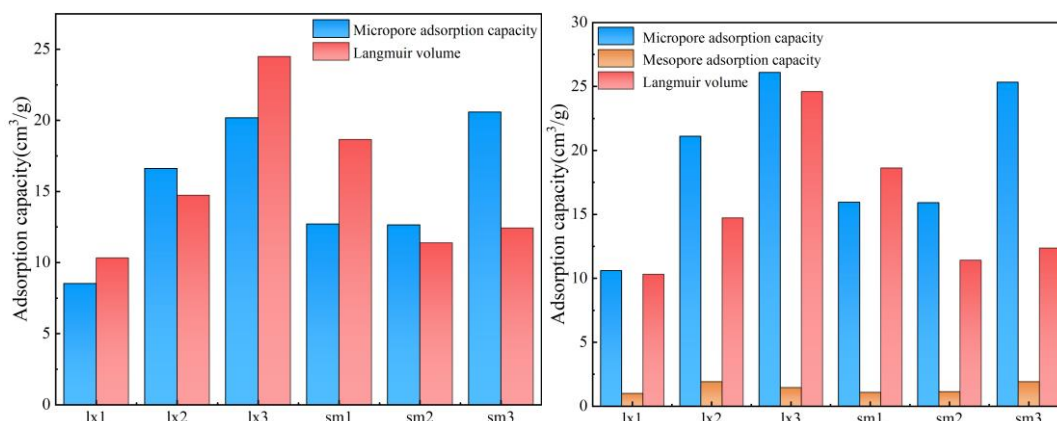


Figure 7. Comparison of adsorption capacity of micropores and mesopores with Langmuir volume (left: Hypothesis I, right: Hypothesis II).

The occurrence characteristics of adsorbed gas are related to the development of pore structure, and the different pore structure results in different occurrence mechanisms. A large number of micropores are developed in the deep coal of the Shenfu-Linxing block. Although the pore volume of micropores is much smaller than that of mesopores, the total pore volume of micropores is relatively high due to the high proportion of micropores and the low content of mesopores, providing sufficient space for the filling of methane molecules [52]. For the shallow and middle reservoirs with relatively low micropore content, there are certain differences in the occurrence mechanism of adsorbed gas. When the volume of micropores is insufficient to accommodate all methane molecules, a portion of them may be stored in mesopores through monomolecular adsorption.

4.4.2. Occurrence Mechanism of Free Gas

Generally, large porosity allows for greater amounts of free gas in the pores. Based on the calculation model for gas content, and considering the actual formation conditions and water saturation characteristics of the Shenfu-Linxing block, the free gas content ranges from 2.03 to 3.26 m³/t, while the adsorbed gas content ranges from 9.58 to 19.16 m³/t. The adsorbed gas content is significantly higher than the free gas content. This is mainly because the deep coal reservoirs in the Shenfu-Linxing block predominantly develop micropores, with a low content of mesopores and macropores, resulting in low free gas content and low gas saturation in coal seams [43,52].

4.5. Phase Evolution of Deep CBM

Through the calculation of gas content in the deep coal, along with the analysis of their occurrence characteristics, it is showed that the adsorbed gas content exhibits a pattern of “rapid growth—slow growth—slow reduction” with increasing burial depth. Conversely, the free gas content follows a pattern of “stable growth—slow growth—gradual stabilization”. The total gas content can be divided into four stages: “rapid growth—slow growth—stable—slow reduction”. Besides the effects of burial depth, temperature, and pressure, the gas content is also influenced by the coal metamorphism degree and water saturation. As the coal metamorphism degree increases, both adsorbed and free gas contents increase [15]. As water saturation rises, the contents of both adsorbed and free gas decline, resulting in a decrease in the overall gas content (Figure 8).

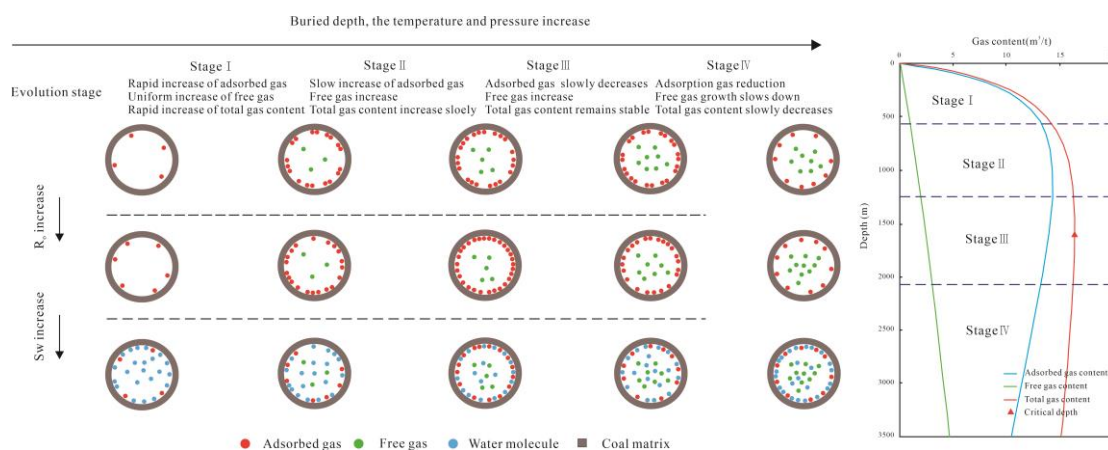


Figure 8. Phase evolution model of deep CBM (modified from [15]).

When the coal burial depth is below 600 m, the total gas content shows a significant upward trend. At this stage, the beneficial effect of pressure on adsorbed gas content surpasses the adverse effect of temperature, leading to a rapid rise in adsorbed gas content as depth increases. Meanwhile, the free gas content, although relatively small, shows a steady increase. Overall, the total gas content displays rapid growth characteristics.

In the depth range of 600 to 1300 m, the total gas content experiences a gradual increase. During this phase, while the positive influence of pressure remains notable, the negative effect of temperature on adsorbed gas content becomes more pronounced. Consequently, the rate of adsorbed gas content growth diminishes. On the other hand, free gas content maintains a consistent upward trend. Overall, the total gas content exhibits characteristics of slow growth during this period.

When the buried depth ranges from 1300 to 2100 m, the total gas content remains stable. At this stage, the adverse effect of temperature on adsorbed gas content surpasses the beneficial influence of pressure, causing a gradual decline in adsorbed gas. Meanwhile, free gas content continues to rise. This equilibrium between declining adsorbed gas and increasing free gas results in the total gas content stabilizing. Typically, this stage marks the appearance of a critical depth.

At depths exceeding 2100 m, the total gas content shows a gradual decline. During this phase, the negative influence of temperature on adsorbed gas content remains dominant, causing a steady reduction in adsorbed gas as depth increases. Concurrently, the proportion of micropores rises, while mesopores and macropores become scarcer, reducing the storage capacity for free gas within the coal seam. As burial depth increases further, the growth rate of free gas content gradually slows down until it stabilizes. Consequently, the total gas content exhibits characteristics of slow reduction during this stage.

5. Conclusions

This study is based on the isothermal adsorption characteristics of deep coal seams, combined with vitrinite reflectance, temperature, pressure, and water saturation parameters, to establish prediction models for coalbed methane content in different phases, revealing the occurrence mechanism of deep coalbed methane, and the following conclusions are drawn.

The adsorption capacity is obviously controlled by the positive effect of pressure in the shallow buried area and is less affected by the temperature. The overall performance is that the buried depth increases and the adsorption capacity increases. In the deep buried area, the adsorption capacity is obviously controlled by the negative effect of temperature.

Based on isothermal adsorption experiments under varying temperature and pressure, and incorporating parameters such as R_o , temperature, pressure, and water saturation, a prediction model for adsorbed and free gas content was constructed with an average error rate of less than 20%. The adsorbed gas content first rises and then declines as burial depth increases, whereas the free gas content grows before eventually leveling off. With higher water saturation, the share of adsorbed gas steadily diminishes, while the proportion of free gas rises.

Adsorbed gas is predominantly stored in coal micropores through a filling mechanism, whereas free gas is largely contained in mesopores and macropores in an unbound state. With increasing burial depth, the total gas content follows a trend of “rapid growth—slow growth—stability—slow reduction”.

Author Contributions: Conceptualization, L.M. and F.Y.; methodology, L.M.; software, L.M.; validation, J.Y. (Jianghao Yang) and S.T.; formal analysis, J.Y. (Jiang Yang) and Y.C.; investigation, L.M.; resources, W.W.; data curation, C.L.; writing—original draft preparation, L.M.; writing—review and editing, F.Y. and S.T.; visualization, B.Z.; supervision, S.T.; project administration, S.T.; funding acquisition, S.T. All authors have read and agreed to the published version of the manuscript.

Funding: This work was financially supported by the National Natural Science Foundation of China (42272200); The Technology Project of Huaneng Group Headquarters (Medium-Deep Low-Rank Coalbed Methane Resource Potential Evaluation and Key Development Technologies of Zhalaينوer Coalfield, HNKJ23-H51); The Science and Technology Major Project of China National Petroleum Corporation (2023ZZ18-03); The Science and Technology Major Project of Changqing Oilfield (2023DZZ01). The authors also thank the reviewers and editors for their constructive comments and suggestions on improving this manuscript.

Data Availability Statement: The data presented in this study are available upon request from the corresponding author due to privacy restrictions.

Acknowledgments: The authors are grateful to the editor and anonymous reviewers for their careful reviews and detailed comments, which helped to substantially improve the manuscript.

Conflicts of Interest: Author Litao Ma, Jianghao Yang, Wei Wang, Cheng Liu, Bo Zhang and Jiang Yang were employed by the company Zhalaينوer Coal Industry Co., Ltd. Author Yi Cui was employed by the company Zhalaينوer Coal Industry Co., Ltd. The remaining authors declare that the research was conducted in the absence of any commercial or financial relationships that could be construed as a potential conflict of interest.

References

1. Tao, S.; Chen, S.D.; Tang, D.Z.; Zhao, X.; Xu, H.; Li, S. Material composition, pore structure and adsorption capacity of low-rank coals around the first coalification jump: A case of eastern Junggar Basin, China. *Fuel* **2018**, *211*, 804–815. [[CrossRef](#)]
2. Xu, H.; Tang, D.; Tao, S.; Li, S.; Tang, S.; Chen, S.; Zong, P.; Dong, Y. Differences in geological conditions of deep and shallow coalbed methane and their formation mechanisms. *Coal Geol. Explor.* **2024**, *52*, 33–39.
3. Chalmers, G.R.L.; Marc Bustin, R. On the effects of petrographic composition on coalbed methane sorption. *Int. J. Coal Geol.* **2007**, *69*, 288–304. [[CrossRef](#)]
4. Tao, S.; Pan, Z.J.; Tang, S.L.; Chen, S.D. Current status and geological conditions for the applicability of CBM drilling technologies in China: A review. *Int. J. Coal Geol.* **2019**, *202*, 95–108. [[CrossRef](#)]
5. Ye, J.C.; Tao, S.; Zhao, S.P.; Li, S.; Chen, S.D.; Cui, Y. Characteristics of methane adsorption/desorption heat and energy with respect to coal rank. *J. Nat. Gas. Sci. Eng.* **2022**, *99*, 104445. [[CrossRef](#)]
6. Qin, Y.; Moore, T.A.; Shen, J.; Yang, Z.B.; Shen, Y.L.; Wang, G. Resources and geology of coalbed methane in China: A review. *Int. Geol. Rev.* **2018**, *60*, 777–812. [[CrossRef](#)]
7. Tao, S.; Tang, D.; Xu, H.; Li, S.; Geng, Y.; Zhao, J.; Wu, S.; Meng, Q.; Kou, X.; Yang, S.; et al. Fluid velocity sensitivity of coal reservoir and its effect on coalbed methane well productivity: A case of Baode Block, northeastern Ordos Basin, China. *J. Pet. Sci. Eng.* **2017**, *152*, 229–237. [[CrossRef](#)]

8. Men, X.Y.; Tao, S.; Liu, Z.X.; Tian, W.G.; Chen, S.D. Experimental study on gas mass transfer process in a heterogeneous coal reservoir. *Fuel Process Technol.* **2021**, *216*, 106779. [[CrossRef](#)]
9. Hou, H.; Shao, L.; Guo, S.; Li, Z.; Zhang, Z.; Yao, M.; Zhao, S.; Yan, C. Evaluation and genetic analysis of coal structures in deep Jiaozuo Coalfield, northern China: Investigation by geophysical logging data. *Fuel* **2017**, *209*, 552–566. [[CrossRef](#)]
10. Li, J.; Wu, Q.; Jin, W.; Lu, J.; Nan, Z. Logging evaluation of free-gas saturation and volume content in Wufeng-Longmaxi organic-rich shales in the Upper Yangtze Platform, China. *Mar. Pet. Geol.* **2019**, *100*, 530–539. [[CrossRef](#)]
11. Tao, S.; Zhao, X.; Tang, D.; Deng, C.; Meng, Q.; Cui, Y. A model for characterizing the continuous distribution of gas storing space in low-rank coals. *Fuel* **2018**, *233*, 552–557. [[CrossRef](#)]
12. Li, Y.; Gao, S.; Wu, P.; Xu, L.; Ma, L.; Hu, W.; Yang, J. Evaluation and correction of the prediction model for free gas content in deep coalbed methane: A Case study of deep coalbed methane in the eastern margin of Ordos Basin. *Acta Pet. Sin.* **2023**, *44*, 1892–1902.
13. Tao, S.; Chen, S.; Pan, Z. Current status, challenges, and policy suggestions for coalbed methane industry development in China: A review. *Energy Sci. Eng.* **2019**, *7*, 1059–1074. [[CrossRef](#)]
14. Xu, H.; Pan, Z.; Hu, B.; Liu, H.; Sun, G. A new approach to estimating coal gas content for deep core sample. *Fuel* **2020**, *277*, 118246. [[CrossRef](#)]
15. Yang, J.; Feng, P.; Tang, S.; Tang, D.; Wang, M.; Li, S.; Zhao, Y.; Li, Z. Phase control factors and content prediction model of deep coalbed methane in Daning-Jixian Block. *Acta Pet. Sin.* **2023**, *44*, 1879–1891.
16. Jing, G.; Chen, Z.; Hui, G. A novel model to determine gas content in naturally fractured shale. *Fuel* **2021**, *306*, 121714. [[CrossRef](#)]
17. Shi, J.; Chang, Y.; Wu, S.; Xiong, X.; Liu, C.; Feng, K. Development of material balance equations for coalbed methane reservoirs considering dewatering process, gas solubility, pore compressibility and matrix shrinkage. *Int. J. Coal Geol.* **2018**, *195*, 200–216. [[CrossRef](#)]
18. Feng, R. A Method to Evaluated Gas Content with Coalbed Methane Reservoir Based on Adsorption Theory and Production Analysis. *Geofluids* **2022**, *1*, 7341886. [[CrossRef](#)]
19. Liu, D.; Yao, Y.; Chang, Y. Measurement of adsorption phase densities with respect to different pressure: Potential application for determination of free and adsorbed methane in coalbed methane reservoir. *Chem. Eng. J.* **2022**, *446*, 137103. [[CrossRef](#)]
20. Wang, Y.; Kang, J.; Zhou, F.; Yuan, L.; Pan, Z. Evaluation of lost gas in the borehole drilling stage: Implication for the direct method of coalbed methane content determination. *J. Nat. Gas. Sci. Eng.* **2022**, *105*, 104711. [[CrossRef](#)]
21. Ji, Y.S.; Ma, D.M.; Chen, Y.; Li, W.B.; Li, G.F.; Zheng, C.; Ma, Z.Y.; Wang, L.Y.; Wang, X. Study on gas content variation and main controlling of low-rank coal in Huanglong Jurassic coalfield. *Energ. Explor. Exploit.* **2023**, *41*, 561–584. [[CrossRef](#)]
22. Xiong, X.; Yan, X.; Xu, F.; Li, S.; Nie, Z.; Feng, Y.; Liu, Y.; Chen, M.; Sun, J.; Zhou, K.; et al. Analysis of multi-factor coupling control mechanism, desorption law and development effect of deep coalbed methane. *Acta Pet. Sin.* **2023**, *44*, 1812–1826+1853.
23. Li, S.; Qin, Y.; Tang, D.; Shen, J.; Wang, J.; Chen, S. A comprehensive review of deep coalbed methane and recent developments in China. *Int. J. Coal Geol.* **2023**, *279*, 104369. [[CrossRef](#)]
24. Xie, Y.G.; Qin, Y.; Meng, S.Z.; Pan, X.Z.; Gao, L.J.; Duan, C.J. Study on occurrence characteristics and controlling factors of Permian Deep Coalbed Methane in Linxing Block. *Fresen Environ. Bull.* **2022**, *31*, 3408–3414.
25. Zhang, Z.; Qin, Y.; Yang, Z.; Li, G.; You, Z. Primary Controlling Factors of Coalbed Methane Well Productivity and High Productive Well Patterns in Eastern Yunnan and Western Guizhou, China. *Nat. Resour. Res.* **2023**, *32*, 2711–2726. [[CrossRef](#)]
26. Cui, S.; Wu, P.; Zhao, F.; Niu, Y.; Cai, W.; Wang, B. Shale Gas Accumulation Factors and Enrichment Area Prediction in Linxing block, Eastern Margin of the Ordos Basin. *Geoscience* **2022**, *36*, 1271–1280.
27. Wang, D.; Cheng, Y.; Yuan, L.; Wang, C.; Wang, L. Implications of Geological Conditions on Gas Contents: A Case Study in the Pingdingshan Coalfield. *Energ. Fuel* **2023**, *37*, 6465–6478. [[CrossRef](#)]
28. Guo, J.; Zhang, Z.; Xiao, H.; Zhang, C.; Zhu, L.; Wang, C. Quantitative interpretation of coal industrial components using a gray system and geophysical logging data: A case study from the Qinshui Basin, China. *Front. Earth Sci.* **2023**, *10*, 1031218. [[CrossRef](#)]
29. Li, Y.; Wang, Z.; Tang, S.; Elsworth, D. Re-evaluating adsorbed and free methane content in coal and its ad- and desorption processes analysis. *Chem. Eng. J.* **2022**, *428*, 131946. [[CrossRef](#)]
30. Pan, Z. Modeling of coal swelling induced by water vapor adsorption. *Front. Chem. Sci. Eng.* **2012**, *6*, 94–103. [[CrossRef](#)]
31. Liu, J.; Chang, S.; Zhang, S.; Li, Y.; Hao, Y.; He, G.; He, Y.; Liu, B. Prediction of coalbed methane content based on seismic identification of key geological parameters: A case in a study area, Southern Qinshui Basin. *Acta Geophys.* **2023**, *71*, 2645–2662. [[CrossRef](#)]
32. Qin, Y.; Song, Q.; Fu, X. Feasibility Study on Co extraction of Coalbed Methane and Conventional Oil and Gas—Adsorption Effect under Equilibrium Water Conditions in Deep Coal Reservoirs. *Nat. Gas. Geosci.* **2005**, *04*, 492–498.
33. Ma, Z.Y.; Tao, S.; Gao, L.C.; Cui, Y.; Jing, Q.H.; Chen, S.D.; He, W.; Guo, J.; Hai, L.F. Detailed Characterization of Microscopic Pore Structure in Low-Rank Coal: A Case Study of Zhalainguoer Coalfield. *Nat. Resour. Res.* **2024**, *33*, 2261–2277. [[CrossRef](#)]
34. Xu, H.; Tang, D.Z.; Liu, D.M.; Tang, S.H.; Yang, F.; Chen, X.Z.; He, W.; Deng, C.M. Study on coalbed methane accumulation characteristics and favorable areas in the Binchang area, southwestern Ordos Basin, China. *Int. J. Coal Geol.* **2012**, *95*, 1–11. [[CrossRef](#)]

35. Tang, X.; Zhang, J.; Shan, Y.; Xiong, J. Upper Paleozoic coal measures and unconventional natural gas systems of the Ordos Basin, China. *Geosci. Front.* **2012**, *3*, 863–873. [[CrossRef](#)]
36. Xue, G.; Liu, H.; Li, W. Deformed coal types and pore characteristics in Hancheng coalmines in Eastern Weibei coalfields. *Int. J. Min. Sci. Technol.* **2012**, *22*, 681–686. [[CrossRef](#)]
37. Chen, H.; Tian, W.; Chen, Z.; Zhang, Q.; Tao, S. Genesis of Coalbed Methane and Its Storage and Seepage Space in Baode Block, Eastern Ordos Basin. *Energies* **2022**, *15*, 81. [[CrossRef](#)]
38. GB/T 30732-2014; Proximate Analysis of Coal. Instrumental Method. Standardization Administration of China: Beijing, China, 2014. (In Chinese)
39. GB/T 8899-2013; Determination of Maceral Group Composition and Minerals in Coal. Standardization Administration of China: Beijing, China, 2013. (In Chinese)
40. GB/T 6948-2008; Method of Determining Microscopically the Reflectance of Vitrinite in Coal. Standardization Administration of China: Beijing, China, 2008. (In Chinese)
41. GB/T 19560-2008; Experimental Method of High-Pressure Isothermal Adsorption to Coal. Standardization Administration of China: Beijing, China, 2008. (In Chinese)
42. Song, D.; Ji, X.; Li, Y.; Zhao, H.; Song, B.; He, K. Heterogeneous development of micropores in medium-high rank coal and its relationship with adsorption capacity. *Int. J. Coal Geol.* **2020**, *226*, 103497. [[CrossRef](#)]
43. Li, H.; Zhou, G.; Chen, S.; Li, S.; Tang, D. In Situ Gas Content and Extraction Potential of Ultra-Deep Coalbed Methane in the Sichuan Basin, China. *Nat. Resour. Res.* **2025**, *34*, 563–579. [[CrossRef](#)]
44. Feng, P.; Li, S.; Tang, S.; Tang, D.; Zhang, C.; Yang, J.; Liu, N.; Zhong, G. Estimation of Adsorption Isotherm for Deep Coalbed Methane: A Monolayer-Filling Model Based on Pore Fractal Dimension. *Energ. Fuel* **2024**, *38*, 1987–2000. [[CrossRef](#)]
45. Feng, P.; Li, S.; Tang, S.; Tang, D.; Zhang, C.; Zhong, G.; Fan, L.; Zhang, Z. Unraveling the Nanopores Evolution: Chemical Structure Control in Coal during Coalification. *Energ. Fuel* **2024**, *38*, 8688–8699. [[CrossRef](#)]
46. Zhang, D.; Cui, Y.; Liu, B.; Li, S.; Song, W.; Lin, W. Supercritical Pure Methane and CO₂ Adsorption on Various Rank Coals of China: Experiments and Modeling. *Energ. Fuel* **2011**, *25*, 1891–1899. [[CrossRef](#)]
47. Krooss, B.M.; van Bergen, F.; Gensterblum, Y.; Siemons, N.; Pagnier, H.J.M.; David, P. High-pressure methane and carbon dioxide adsorption on dry and moisture-equilibrated Pennsylvanian coals. *Int. J. Coal Geol.* **2002**, *51*, 69–92. [[CrossRef](#)]
48. Wang, Q.; Shen, J.; Glover, P.; Lorinczi, P.; Duncan, I. Improving the Prediction of Production Loss in Heterogeneous Tight Gas Reservoirs Using Dynamic Threshold Pressure. *Energ. Fuel* **2022**, *36*, 11991–12003. [[CrossRef](#)]
49. Ma, X.; Song, Y.; Liu, S.; Jiang, L.; Hong, F. Quantitative research on adsorption capacity evolution of medium-high rank coal reservoirs in geological history: A case study from Hancheng area in the Ordos Basin. *Acta Pet. Sin.* **2014**, *35*, 1080–1086.
50. Wu, J.; Tang, D.; Li, S.; Ren, P. Characteristics and influence factors of pore structure of coal reservoirs in the eastern margin of Ordos basin. *Coal Geol. Explor.* **2017**, *45*, 58–65.
51. Fu, X.; Qin, Y.; Wang, G.G.X.; Rudolph, V. Evaluation of gas content of coalbed methane reservoirs with the aid of geophysical logging technology. *Fuel* **2009**, *88*, 2269–2277. [[CrossRef](#)]
52. Ge, X.; Liu, D.; Cai, Y.; Wang, Y. Gas Content Evaluation of Coalbed Methane Reservoir in the Fukang Area of Southern Junggar Basin, Northwest China by Multiple Geophysical Logging Methods. *Energies* **2018**, *11*, 1867. [[CrossRef](#)]

Disclaimer/Publisher’s Note: The statements, opinions and data contained in all publications are solely those of the individual author(s) and contributor(s) and not of MDPI and/or the editor(s). MDPI and/or the editor(s) disclaim responsibility for any injury to people or property resulting from any ideas, methods, instructions or products referred to in the content.